Palaeogeography, Palaeoclimatology, Palaeoecology 699 (2026) 113983

Contents lists available at ScienceDirect

Palaeogeography, Palaeoclimatology, Palaeoecology

journal homepage: www.elsevier.com/locate/palaeo

Early Pleistocene (~2.6 Ma) birth of the modern Huai River through borehole-based provenance analysis (Subei Basin, eastern China)☆

Yingdi Pan [a,1], Tao Deng [a,1], Junpeng Guan [b,c], Lijuan Wang [b,c], Eduardo Garzanti [d], Xiumian Hu [a,*]

[a] State Key Laboratory of Critical Earth Material Cycling and Mineral Deposits, Key Laboratory of Surficial Geochemistry, Ministry of Education, School of Earth Sciences and Engineering, Nanjing University, Nanjing 210023, China
[b] Geological Survey of Jiangsu Province, Nanjing 210018, Jiangsu Province, China
[c] Natural Resources Carbon Neutralization Engineering Research Center of Jiangsu Province, Nanjing 210018, Jiangsu Province, China
[d] Laboratory for Provenance Studies, Department of Earth and Environmental Sciences, University of Milano–Bicocca, 20126 Milano, Italy

ARTICLE INFO

Editor: Howard Falcon-Lang

Keywords:
Subei Basin
Detrital zircon
Multi-proxy provenance
Huai River

ABSTRACT

The origin and evolution of the Huai River remain controversial. Previous studies have largely focused on the middle and upper reaches, where incomplete stratigraphic records prevent to obtain accurate constraints. The Subei Basin, as the largest Cenozoic depocenter of the Huai River, provides a perfectly suitable archive for reconstructing drainage evolution. This study presents a systematic provenance analysis of siliciclastic rocks from the Sure wells, integrating sandstone petrography and detrital zircon U-Pb geochronology. Results reveal that: 1) during the Late Cretaceous–Paleogene, the Subei Basin received sediments predominantly from local sources, including the Zhangbaling and Sunan uplifts in the south; 2) during the Neogene, sediments sourced from the Jinsha (upper Yangtze) drainage area appeared in the basin – as testified by basaltic rock fragments and diagnostic Cenozoic zircons derived from the southeastern margin of the Tibetan Plateau – marking the initial development of the Paleo-Yangtze River system; 3) since the Early Pleistocene (~2.6 Ma), a sharp increase in metamorphic lithic fragments and 200–350 Ma metamorphic zircons indicate provenance from the Qinling-Dabie orogen, signaling the initial establishment of the modern Huai drainage. This study provides new constraints on the birth of the Huai River from a sink perspective and offers important insights into the Cenozoic drainage evolution of eastern China.

1. Introduction

The Huai River flows ~1100 km eastward from the Tongbai Mountains along the northern piedmont of the Tongbai-Dabie orogen, serving as a critical geographical and climatic boundary in eastern China (Fig. 1; Deng et al., 2024). Despite its significance, research on its formation lags far behind that of the Yangtze and Yellow Rivers (Zheng et al., 2013; Hu et al., 2017). The timing of the birth of the modern Huai River remains particularly contentious, with estimates spanning the early to late Pleistocene. The evidence underlying these divergent views thus requires critical examination.

Existing constraints on drainage formation derive from three principal lines of evidence (i.e., paleochannel/geomorphology, stratigraphy/sedimentology, and provenance), each with distinct limitations. 1) Geomorphic studies have identified stepped planation surfaces and river terraces in the middle and upper reaches, proposing an early–middle Pleistocene formation age (e.g., Li et al., 2020). However, these surfaces generally lack chronological control, and the terrace record is incomplete and discontinuous due to active tectonic uplift (Shi et al., 2019). Consequently, it remains unclear whether these landforms record the initial drainage integration or later modifications. 2) Stratigraphic studies document a basin-wide transition from lacustrine to fluvial facies, constraining the establishment of a through-going river to either the early Pleistocene (~1.7 Ma) or middle–late Pleistocene (0.73–0.13 Ma) (Zuo et al., 2006; Zhang et al., 2018). However, such a facies shift is non-unique—it can also be driven by aridification, tectonic

☆ This article is part of a Special issue entitled: 'Cenozoic topographic evolution' published in Palaeogeography, Palaeoclimatology, Palaeoecology.

* Corresponding author.
E-mail address: huxm@nju.edu.cn (X. Hu).

[1] These authors contributed equally.

https://doi.org/10.1016/j.palaeo.2026.113983
Received 26 January 2026; Received in revised form 16 June 2026; Accepted 17 June 2026
Available online 18 June 2026

tilting, or base-level fall (Carroll and Bohacs, 1999). Thus, a key unresolved question is whether the observed facies transition indeed records drainage integration or instead reflects other environmental changes. 3) Provenance studies using heavy minerals, garnet geochemistry, and detrital zircon geochronology have demonstrated the sensitivity of the Subei Basin to drainage reorganization (Chen, 2014; Zhang, 2016; Tao, 2022). However, most of these studies relied on single-proxy approaches and short time windows (mostly Pliocene–Pleistocene), yielding divergent conclusions on the timing of Huai River formation. Hence, a second unresolved question is the precise timing and full evolutionary trajectory of the river integration event.

To address these questions, this study implements a long-term, multi-proxy provenance strategy in the Subei Basin—the primary Cenozoic sink of the Huai River. Benefiting from sustained subsidence since the Late Cretaceous, the basin's Dongtai Depression preserves a thick (>6000 m) and uninterrupted sedimentary succession (Qiu et al., 2006a, 2006b), making it an ideal archive to reconstruct a complete drainage history. Unlike sedimentological facies analysis, which is inherently equivocal, provenance proxies directly track sediment routing systems. Specifically, a stratigraphic shift from localized sources (e.g., adjacent uplifts) to distal source terranes (e.g., the Qinling-Dabie orogen) provides unambiguous evidence for large-scale river integration, independent of climatic or local tectonic influences.

Here, we integrate sandstone petrography, detrital zircon U-Pb geochronology, and zircon trace-element geochemistry from the Sure-1 and Sure-2 drill cores, establishing a robust, continuous provenance framework extending to the Lower Pleistocene. Constrained by a well-established magnetostratigraphic and OSL chronology, our systematic dataset aims to: 1) identify the exact timing and nature of key provenance shifts that mark major drainage reorganizations; and 2) provide independent, sink-based constraints to resolve the longstanding controversy surrounding the birth of the modern Huai River.

2. Geological setting

2.1. Subei Basin

The Subei Basin (SB) is situated to the north of the Yangtze Delta and constitutes the onshore segment of the Subei-South Yellow Sea Basin, spanning an area exceeding 30,000 km^2 (Fig. 2). The SB, a typical fault-bound basin (Wang et al., 2008; Cheng et al., 2019), straddles the northeastern edge of the Yangtze Block, delimited by the Tanlu Fault to the west, the Yellow Sea to the east, the Sulu Orogenic Belt to the north, and the Sunan Uplift to the south (Yang and Chen, 2003). Since the Late Cretaceous, East China experienced tectonic extension and formation of several rift basins, including the SB (Ren et al., 2002; Shu et al., 2021). Intensified rift tectonics allowed the accumulation of thick fluvial sediments in the SB during the Paleogene (Lin et al., 2004), followed by transition from a localized fault depression to an open basin in the Neogene (Zhu et al., 2020). The basin expanded further and siliciclastic sediments continued to accumulate in the Quaternary, when the depocenter gradually shifted southward toward the modern Yangtze mouth, eventually leading to the formation of the tide-dominated Yangtze River Delta (Wang et al., 2006; Shu et al., 2021).

2.2. Stratigraphy

The sedimentary sequence of the Subei Basin consists of several-km-thick Paleogene strata, overlain by over 1-km-thick Neogene strata capped by Quaternary deposits ranging from 50 to 300 m in thickness (Cheng et al., 2019; Shu et al., 2021). The succession includes the Pukou, Taizhou, Funing, Dainan, Sanduo, Yancheng and Wuduizhen formations. The Upper Cretaceous Pukou Formation (K_2p) is subdivided into three members (Fig. 3). The lower member mostly consists of lacustrine deposits including reddish-brown to gray mudrocks and fine sandstones, the middle member of fluvial deposits including light gray conglomerate and brown to reddish-brown mudrocks, and the upper member of lacustrine deposits including reddish-brown to light gray, locally gypsum-bearing mudrocks.

The Paleocene Taizhou Formation (E_1t) mostly consists of light brown sandstone and dark gray mudrock, with intercalated lacustrine oolitic limestone and grayish-black mudstone up-section. The Paleocene Funing Formation (E_1f) documents a fining-upward sequence with dark brown fluvial sandstone and dark gray mudrock passing up-section to grayish-black lacustrine shale and light-colored siltstone with interbedded basaltic lavas (Cai et al., 2019; Peng et al., 2020).

The Eocene Dainan Formation (E_2d), increasing in thickness from west to east, mainly consists of light gray sandstone and varicolored

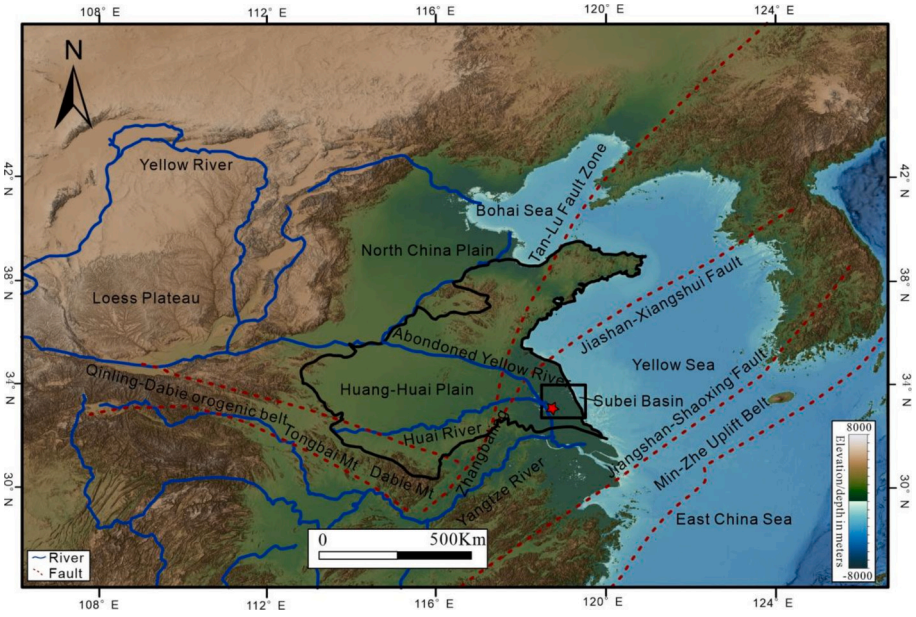

Fig. 1. Topographic map of East Asia, showing major rivers and locations mentioned in text. Image is based on ETOPO1 global relief model sourced from the National Geophysical Data Center of the National Oceanic and Atmospheric Administration (https://www.ngdc.noaa.gov). Black polygon outlines the boundary of the Huai River Basin (Resource and Environmental Science Data Center of the Chinese Academy of Sciences, http://www.resdc.cn).

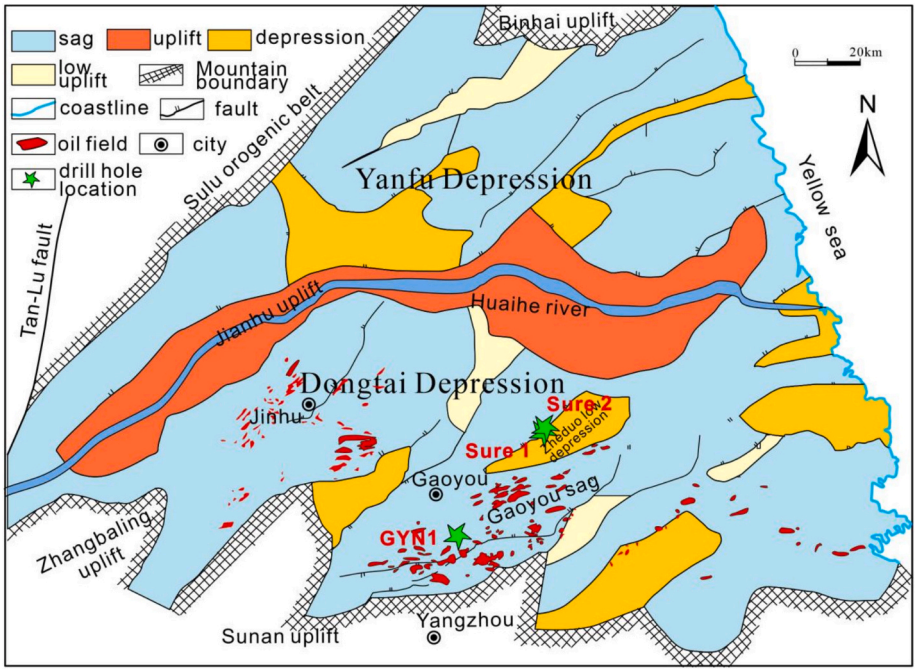

Fig. 2. Tectonic map of the Subei Basin (mod. after Qiu et al., 2006a, 2006b).

mudrock layers with dark lower part and reddish upper part. The Eocene Sanduo Formation (E_2s) mostly consists of brownish-red mudrocks; several basalt layers encountered in the GYN1 Well yielded Eocene $^{40}Ar/^{39}Ar$ ages between 44 Ma and 41 Ma (Tao, 2022).

The Neogene Yancheng Formation ($N_{1\text{-}2}y$) is subdivided into two members. The Miocene lower member (N_2y^1) consists of grayish-white and brownish-gray sandstones and conglomerates interbedded with dark brownish-red lacustrine mudrocks. The Pliocene upper member (N_2y^2; basal boundary ~5.3 Ma; Tao, 2022) comprises grayish-white and brownish-gray coarse fluvial sandstone and sandy conglomerate interbedded with varicolored clay.

The Pleistocene Wuduizhen Formation is dominated by yellowish-green mudrocks with abundant calcareous concretions and locally interbedded medium to coarse fluvial sandstones, (Fig. 3). The base of this unit was constrained as ~2.6 Ma by Tao (2022), based on correlations with the GYN1 and ZKY04 wells (Liang, 2018) (Fig. 3). Recent deposits consist of unconsolidated gravelly to silty sands.

The Sure-1 and Sure-2 wells located in the Zheduo sag, a secondary structural unit within the Dongtai depression, penetrated strata ranging from Cambrian to Quaternary in age. Cambrian to Ordovician strata mostly consist of dolomite and limestone serving as excellent geothermal reservoirs. The relatively complete continental Cretaceous to Quaternary succession is most suitable for provenance analysis and the proximity to the GYN1 well (~ 60 km apart) allows for a reliable stratigraphic correlation.

2.3. Huai River

The Huai River, the largest by far between the Yellow and Yangtze courses in eastern China (Fig. 1), flows along the northern margin of the Tongbai-Dabie orogenic belt and traverses the Henan, Anhui, and Jiangsu provinces before flowing into the Yangtze River at Sanjiangying (near Yangzhou). The catchment, bounded by the Yellow River to the north, the eastern extension of the Qinling Mountains to the west, and the Tongbai-Dabie and Zhangbaling mountain ranges to the south includes lakes and depressions along both sides of the main channel, forming an asymmetric fan-shaped pattern (Fig. 1). The mountain catchment extends as far Changtaiguan (near Xinyang), whereas the lowland catchment in the Huang-Huai Plain downstream includes low hills in the Bagong area. U-Pb age spectra of zircon grains in modern Huai River sediments are characterized by peaks at 134 Ma, 294 Ma, 466 Ma, and 1874 Ma, along with minor Neoproterozoic and Paleoproterozoic clusters (He, 2014).

2.4. Abandoned Yellow River

The Yellow River, which presently discharges into the Bohai Sea (Fig. 1), is well known for its exceptionally high sediment load (Tregear, 1965; Van Maren et al., 2009). Through much of the Cenozoic, the Yellow River repeatedly shifted southward, transporting into the Subei Basin loess-derived material from the Loess Plateau (Xiong et al., 2024). Notably, between 1128 and 1855 CE (Common Era), the river flowed southward and discharged into the sea via the Abandoned Yellow River Delta (Zhou et al., 2014). Abandoned Yellow River sediments have geochemical composition and heavy-mineral assemblages distinct from those of the modern Yellow River (Gao et al., 2015) and are adopted in our provenance analysis of Subei Basin Cenozoic deposits as a key endmember representative of Yellow River contribution. Its detrital-zircon age spectrum is characterized by dominant peaks at 272 Ma, 455 Ma, and 1859 Ma, along with clusters around 1011 Ma and 2460 Ma (He, 2014).

2.5. Yangtze River

The modern Yangtze River is sourced from the Tibetan Plateau, flows eastward through deep valleys into the Sichuan Basin (Fig. 1), incises the Three Gorges, enters the Jianghan Basin, and ultimately discharges into the East China Sea. The upper reaches upstream of Yichang include metamorphic basement, Paleozoic carbonates, Permian Emeishan basalts, and Cenozoic magmatic rocks. The middle and lower reaches include Paleozoic and Mesozoic continental and marine sedimentary rocks, with mainly felsic magmatic rocks (Yu et al., 2009). The detrital-zircon age spectrum of modern Yangtze sand is characterized by peaks at 213 Ma and 779 Ma, and clusters around 436 Ma, 1860 Ma, and 2479 Ma (He, 2014).

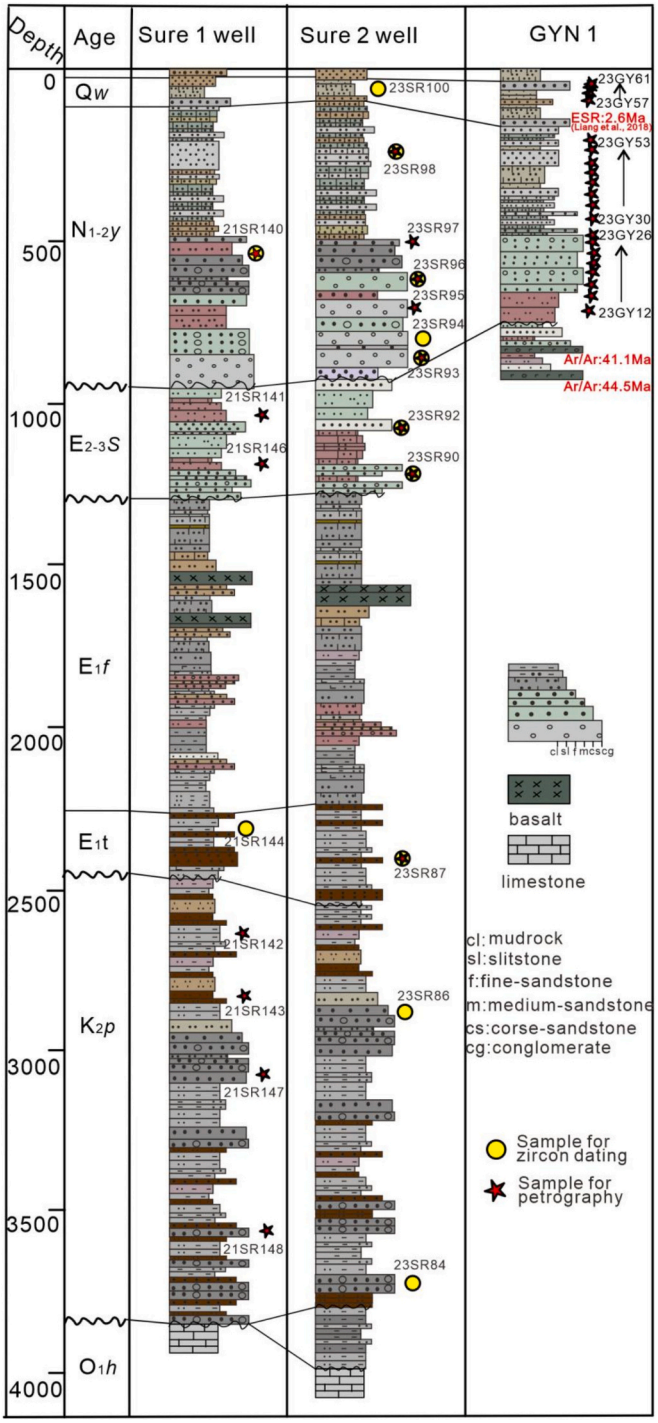

Fig. 3. Stratigraphic correlation of Sure-1, Sure-2, and GYN1 wells, all located in the Dongtai depression ~60 km apart (Fig. 2). Data for GYN1 well from Tao (2022). ESR = Electron spin resonance dating. O_1h = Lower Ordovician Honghuayuan Formation.

3. Samples and methods

Overall, 35 sandstone samples were collected from the Sure-1, Sure-2, and GYN1 wells for petrographic analysis; 12 samples were selected for detrital-zircon U-Pb dating. Full information on sampling locations is provided in Appendix Table S1. In each sample, at least 400 grains were identified as quartz, feldspar, rock fragments or matrix under the petrographic microscope following the Gazzi-Dickinson point-counting method (Ingersoll et al., 1984; Table S1). Accessory and authigenic minerals were not considered. Sandstone classification follows Garzanti (2019).

Zircon grains were separated by standard methods including jaw crushing, water table, magnetic separator and heavy-liquids. Zircons were hand-picked, mounted in epoxy, and ground and polished to half-thickness to expose grain interiors. U-Pb dating was conducted by LA-ICP-MS in the Hongchuang Exploration Technology Service Co., Ltd., Nanjing, China. Laser ablation employed a Resolution SE model (Applied Spectra, USA) equipped with an ATL (ATLEX 300) excimer laser and a two-volume S155 ablation cell. The laser ablation system was coupled to an Agilent 7900 quadrupole (Q)-ICP-MS (Agilent, USA). All analyses were conducted with a laser beam diameter of 30 μm, a 5 Hz pulse frequency, and a fluence of 2.5 J/cm^2. GJ-1 was used as the primary zircon age reference material (Jackson et al., 2004). As secondary age reference material, 91500 was analyzed during every U-Pb run for quality control, obtaining a weighted average $^{206}Pb/^{238}U$ age of 1066.9 ± 7.5 Ma. Data reduction was carried out using *VizualAge* (U–Th–Pb) (Chew et al., 2014) and *Trace_Elements* data reduction schemes, operated with *IOLITE* software package (Paton et al., 2010). The $^{206}Pb/^{238}U$ and $^{207}Pb/^{206}Pb$ ages were used for grains younger and older than 1000 Ma, respectively, both expressed with 2σ uncertainties. A 10% discordance filter [($^{206}Pb/^{238}U$-$^{207}Pb/^{206}Pb$)/$^{207}Pb/^{206}Pb$] was applied for ages >400 Ma. The toolset *detritalPy* was used to generate U-Pb age histograms and kernel density estimates (Sharman et al., 2018). U-Pb dating and trace-element analysis were undertaken on 1635 zircon grains, 1573 of which passed the concordance threshold. Detrital-zircon ages and trace-element data are presented in Appendix Tables S2 and S3.

4. Results

4.1. Sandstone petrography

Sandstones in the Upper Cretaceous Pukou Formation are mostly feldspatho-litho-quartzose with felsic volcanic and subordinate low-rank metamorphic lithics (averages Q:F:L 69:11:20 and Lv:Ls:Lm 77:10:13, Fig. 5). Paleocene sandstones in the Taizhou Formation are also mainly feldspatho-litho-quartzose with felsic volcanic and subordinate carbonate and siltstone lithic fragments (averages Q:F:L 67:10:23 and Lv:Ls:Lm 54:35:11, Fig. 5). Eocene sandstones of the Sanduo Formation are again mostly feldspatho-litho-quartzose with felsic volcanic and subordinate siltstone and shale lithics; embayed quartz grains and a few mafic volcanic rock fragments also occur (averages Q:F:L 60:18:22 and Lv:Ls:Lm 56:26:18). (Fig. 4b).

The Neogene Yancheng Formation contains feldspatho-litho-quartzose sandstones with felsic volcanic lithics, but with more sedimentary, intermediate to mafic volcanic, and low-rank metamorphic lithics (averages Q:F:L 54:12:34 and Lv:Ls:Lm 44:28:28; Fig. 4c,d,e). The Pleistocene Wuduizhen Formation contains litho-feldspatho-quartzose sandstones with a larger variety of lithics types (averages Q:F:L 47:33:20 and Lv:Ls:Lm 42:30:28), Figs. 4f and 5).

4.2. Detrital-zircon U-Pb geochronology

Detrital-zircon dating was conducted on 12 sandstones, including 2 samples from Sure 1 Well (21SR144 and 21SR140) and 10 samples from Sure 2 Well.

4.2.1. Upper Cretaceous Pukou Fm

Sample 23SR84 yielded mostly Paleoproterozoic (~39%) and Neoproterozoic (~23%) populations, with subordinate late Paleozoic (~8%), Triassic (~7%), and Jurassic (~9%) components; ages range from 146 ± 1 Ma to 2576 ± 26 Ma (Fig. 6; Table S2). Sample 23SR86, instead, yielded a predominant Cretaceous population (~25%), with late Paleozoic (~14%), Neoproterozoic (~21%), and Paleoproterozoic (~13%) components; ages range from 76 ± 1 Ma to 2679 ± 19 Ma.

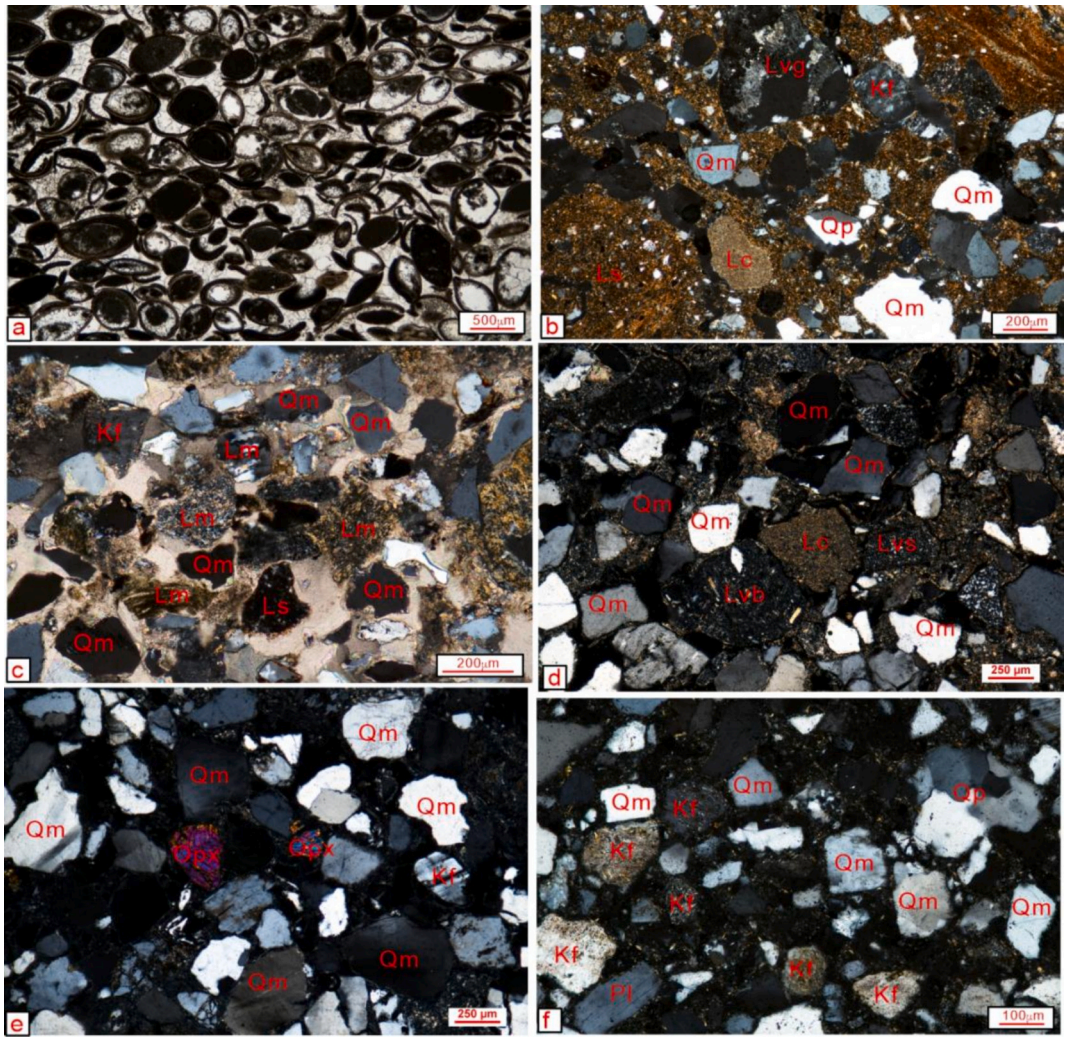

Fig. 4. Microphotographs under cross-polarizing light: a) ostracod biosparite (Taizhou Fm.); feldspatho-litho-quartzose sandstones in the Sanduo (b) and Yancheng Fms. (c: Sure 2 Well; d, e: GYN1 well); f) litho-feldspatho-quartzose sandstone in the Wuduizhen Fm. Qm and Qp = monocrystalline and polycrystalline quartz; Lm, Lvs, and Lvb = metamorphic, felsic volcanic, and intermediate-mafic volcanic lithics. Lvg = granitic rock fragment.

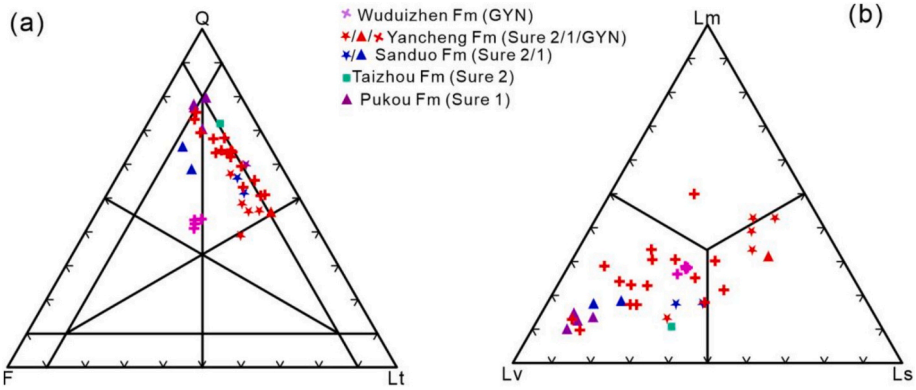

Fig. 5. Sandstone petrography of Sure-1, Sure-2, and GYN1 wells: a) Q = quartz, F = feldspar, L = lithic fragments; b) Lm = metamorphic, Ls = sedimentary, Lv = volcanic lithic fragments.

4.2.2. Paleocene Taizhou Fm

Sample 21SR144 yielded Cretaceous (~14%), Triassic (~14%), late Paleozoic (~18%), Neoproterozoic (~17%) and Paleoproterozoic (~21%) populations; ages range widely from 72 ± 2 Ma to 3060 ± 17 Ma (Fig. 6; Table S2). Sample 23SR87 yielded mainly Paleoproterozoic zircons (~49%), associated with Archean (~8%), late Paleozoic (~17%), Triassic (~5%), and Cretaceous (~7%) components; ages range from 124 ± 1 Ma to 2545 ± 13 Ma.

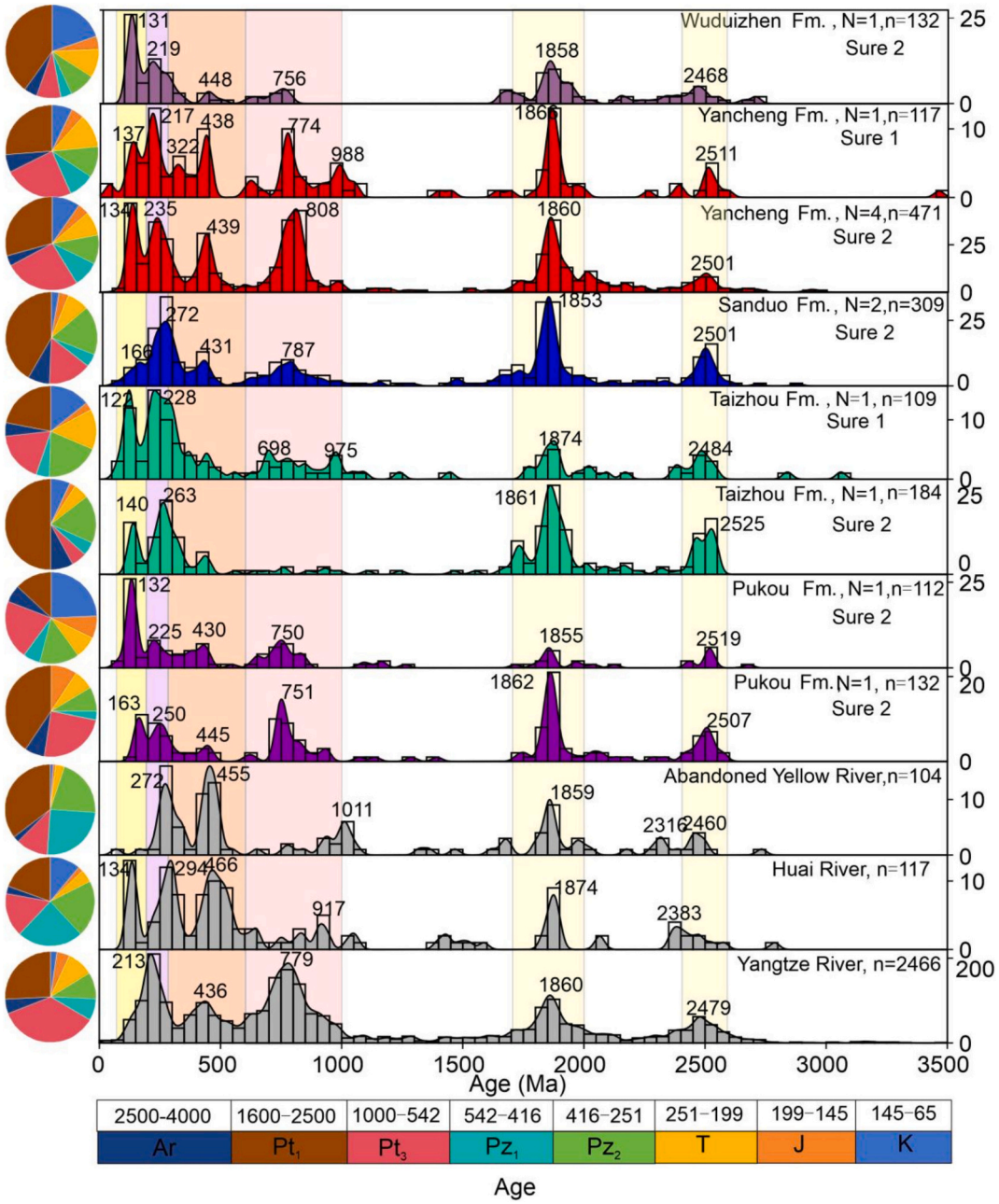

Fig. 6. Normalized U-Pb spectra of detrital zircons from the Subei Basin (proportions of age groups shown as pie charts). Data sources: Huai River and Abandoned Yellow River from He (2014); Yangtze River from Wang et al. (2023a, 2023b). N = number of samples, n = number of zircon grains. (For interpretation of the references to colour in this figure legend, the reader is referred to the web version of this article.)

4.2.3. Eocene Sanduo Fm

Sample 23SR90 also yielded mainly Paleoproterozoic zircons (~42%), associated with Archean (~8%), Neoproterozoic (~11%), and late Paleozoic (~21%) components; ages vary from 83 ± 1 Ma to 2611 ± 20 Ma (Fig. 6; Table S2). Sample 23SR92 yielded a similar spectrum, with mainly Paleoproterozoic zircons (~37%) associated with Archean (~6%), Neoproterozoic (~20%), late Paleozoic (~10%), and Triassic (~11%) components; ages vary from 63 ± 1 Ma to 2881 ± 28 Ma.

4.2.4. Neogene Yancheng Fm

Sample 21SR140 yielded mainly Paleoproterozoic (~25%) and Neoproterozoic (~23%) zircons, associated with early Paleozoic (~9%), late Paleozoic (~10%), Triassic (~11%), and Cretaceous (~7%) components; ages range from 36 ± 1 Ma to 3462 ± 40 Ma. (Fig. 6; Table S2). Samples 23SR93, 23SR94, 23SR96 and 23SR98 yielded similar spectra dominated by Paleoproterozoic (~29%) and Neoproterozoic (~25%) ages with minor Early Paleozoic, Late Paleozoic, Triassic, and Cretaceous components; ages range from 73 ± 1 Ma to 3551 ± 14 Ma.

4.2.5. Pleistocene Wuduizhen Fm

Sample 23SR100 yielded mainly Paleoproterozoic zircons (~40%), associated with Neoproterozoic (~8%), late Paleozoic (~9%), and Cretaceous (~20%) components; ages range from 63 ± 1 Ma to 2881 ± 28 Ma. (Fig. 6; Table S2).

4.3. Zircon geochemistry

The Th/U ratio can be used to identify the origin of zircon grains: metamorphic zircons typically exhibit Th/U < 0.1, whereas most magmatic zircons contain more Th and U, with Th/U > 0.4 (Xiang et al.,

2011; Yakymchuk et al., 2018; Deng et al., 2024). In the 12 analyzed samples, zircon grains display Th/U ratios ranging between 0.1 and 3, ~70% of them indicating magmatic affinity (i.e., Th/U > 0.4), ~23% falling in the transitional range 0.1 < Th/U < 0.4, and only ~6% pointing at metamorphic origin (i.e., Th/U < 0.1; Fig. 7).

Given that the 200–350 Ma age range corresponds to the typical timing of metamorphic events in the Tongbai-Dabie orogen, which represents the headwater region of the Huai River, we examined the trace element compositions of zircons within this specific age interval to assess their metamorphic affinity (Liu et al., 2008; Liu and Liou, 2011). Within the 200–350 Ma age population, zircons with Th/U < 0.1 are 12% in the Pukou Fm. (samples 23SR84 and 23SR86), 10% in the Taizhou Fm. (23SR87, 21SR144), ~6% in the Sanduo Fm., ~7% in the Yancheng Fm., and raise to 24% in the Wuduizhen Formation. Zircons of

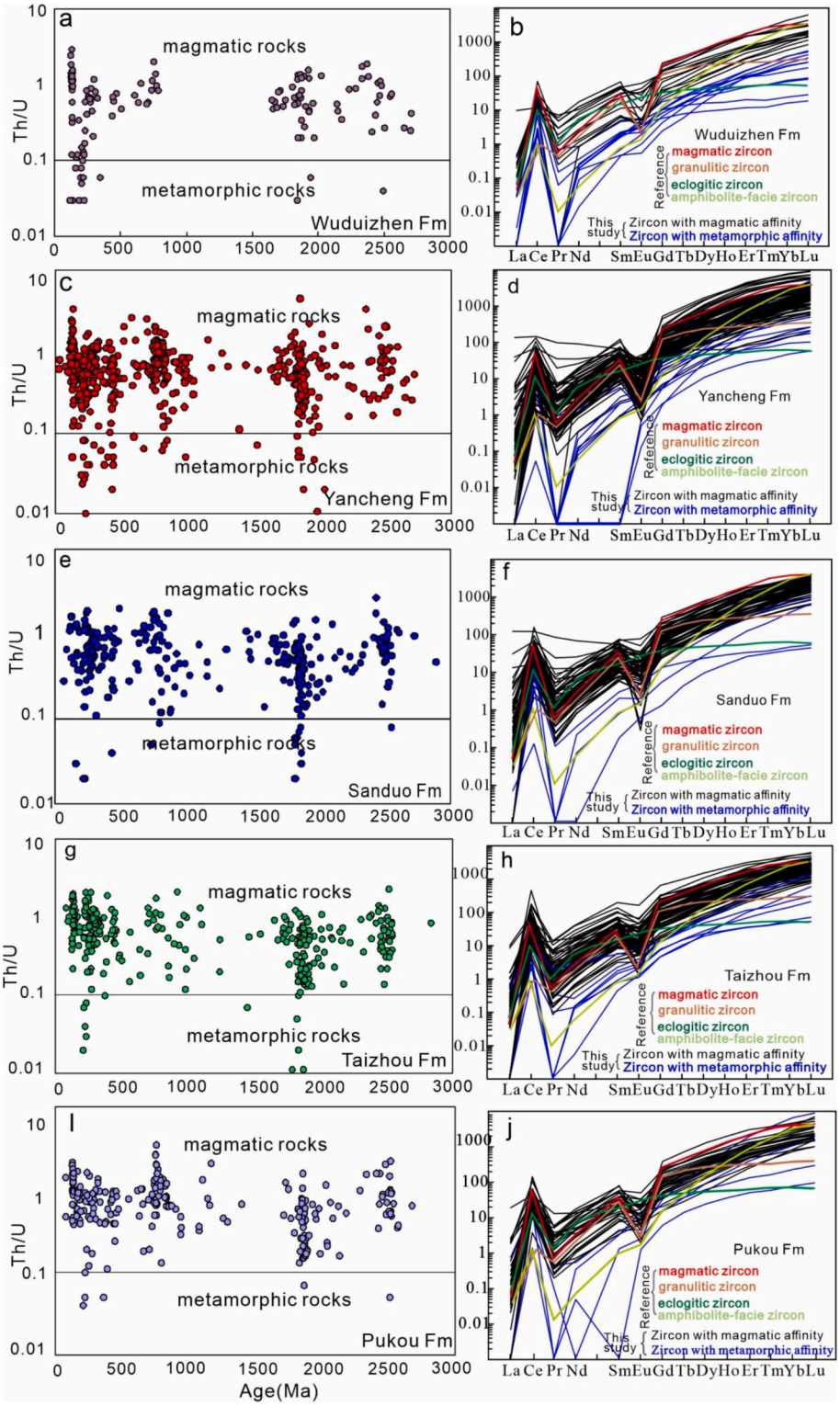

Fig. 7. Trace elements in detrital zircon: (a, c, e, g, i) U-Pb age vs. Th/U ratio; (b, d, f, h, j) chondrite-normalized REE patterns for studied zircons in the 200–350 Ma age range, compared with REE patterns for eclogite-, granulite- and amphibolite-facies zircons (Rubatto, 2017). Chondrite data after Sun and McDonough (1989).

metamorphic affinity have very low Th (from 0.4 to 53.7 ppm) and show no to weak negative Eu anomalies (mostly Eu/Eu* 0.8–1.2, only a few grains reaching down to 0.5), all typical features of metamorphic zircon (Rubatto, 2017).

5. Discussion

5.1. Provenance analysis

Previous provenance studies of the Subei Basin succession have identified five potential source areas (Fig. 2): 1) the Dabie orogen in the west and the eastern segment of the Tan-Lu fault zone, characterized by Proterozoic metamorphic and volcanic rocks; 2) the Binhai Uplift in the north (Lianyungang area), composed mainly of Proterozoic medium/high-grade metamorphic rocks and Paleozoic sedimentary rocks (Shu et al., 2005); 3) the Sulu orogenic belt in the north-east, dominated by metamorphic rocks and Mesozoic igneous rocks (Zheng et al., 2014), which experienced significant uplift at 55–50 Ma and 38–25 Ma (Xu et al., 2022); 4) the Zhangbaling Uplift in the south-west, characterized by Neoproterozoic metamorphic rocks and Mesozoic igneous rocks, with detrital-zircon populations dominated by Neoproterozoic and subordinate Mesozoic ages (Wang et al., 2023a, 2023b); 5) the Sunan Uplift in the south, exposing Sinian carbonate rocks, Paleozoic carbonate and clastic rocks, and Yanshanian intermediate to felsic igneous rocks (Shu et al., 2005).

Sandstones in the Upper Cretaceous Pukou Formation contain abundant felsic volcanic lithics and detrital zircons yielding Jurassic–Cretaceous ages. The lack of (ultra)high-pressure metamorphic rock fragments precludes provenance from the Sulu orogenic belt, which is characterized by widespread ultrahigh-pressure (UHP) metamorphic rocks, including eclogite, garnet peridotite, and jadeite quartzite, formed during the Triassic continental collision (Liu et al., 2008; Liu and Liou, 2011; Zheng et al., 2019). Similarly, the Qinling–Dabie belt contributed only as a minor source, as indicated by the low proportion of metamorphic zircons within the 200–350 Ma age range. Gravel composition in the southern Gaoyou Sag, coupled with downstream fining away from the Sunan Uplift (Wang and Jiang, 2021a, 2021b), point at the Sunan Uplift as the main sediment source, consistently with our petrographic results. The Neoproterozoic metamorphic rocks and Mesozoic igneous rocks widely exposed in the Zhangbaling Uplift represent an alternative source. Petrographic composition and age spectra of detrital zircons in the Taizhou Formation are similar, indicating unchanged provenance from the Sunan and/or Zhangbaling uplifts in the south during the Paleogene.

In the Eocene Sanduo Formation, sedimentary lithics increase moderately, mainly at the expense of felsic volcanic lithics, and detrital zircons yielded mostly Permian and Paleoproterozoic ages. Provenance from a northern area was suggested based on southward decreasing thickness and grain size of sandstone beds in the Gaoyou Sag (Liu et al., 2014). The Binhai Uplift, widely exposing Proterozoic medium/high-grade metamorphic and Paleozoic sedimentary rocks, is indicated as the main sediment source by the excellent match between detrital-zircon age spectra. Some Jurassic zircon ages and carbonate rock fragments hint at additional input from Mesozoic magmatic rocks of the Zhangbaling and/or Sunan uplifts. The Sulu and Dabie orogenic belts are ruled out as major sources because: (1) Cretaceous granitoids dominate these belts yet our samples lack Cretaceous detrital signatures (Zhao et al., 2017); (2) Jurassic granitoids are of limited areal extent in the Sulu orogenic belt and are intimately associated with UHP/HP metamorphic rocks; both the Sulu and Dabie orogenic belts are characterized by widespread UHP/HP metamorphic assemblages (Zhao and Zheng, 2009; Zhao et al., 2017). However, UHP/HP metamorphic rock fragments are rarely observed in our sandstone samples. Thus, the Jurassic zircons are more likely derived from the Zhangbaling and/or Sunan uplifts, which lack UHP assemblages.

In the Neogene Yancheng Formation, supply from Neoproterozoic metamorphic rocks of the Zhangbaling Uplift is indicated by the increased proportion of Early Paleozoic and Neoproterozoic zircon ages, whereas input from Sinian and Paleozoic carbonate rocks widely exposed in the Sunan Uplift is suggested by significant carbonate detritus. An additional potential source is represented by the Jianhu Uplift, a long-term exposed basement high since the late Eocene that separates the Subei Basin into the northern Yanfu depression and southern Dongtai depression (Fig. 2; Shu et al., 2005). Its basement is composed predominantly of medium-acidic igneous rocks, quartzite, and granite (Wang and Jiang, 2021a, 2021b), distinctly different from the UHP metamorphic assemblages of the Dabie-Sulu orogenic belt. Tectonically uplifted in the late Eocene, it blocked sediment supply from the north and shed detritus both to the Yanfu and Dongtai depressions (Fig. 2; Shu et al., 2005). An additional contribution from the upper Yangtze Block is suggested by basaltic rock fragments and minor Cenozoic magmatic zircons in sample 21SR144 from the Sure-1 Well, inferred to be derived from Permian Emeishan continental flood basalts exposed along the western margin of the Sichuan Basin and from intermediate to felsic Cenozoic magmatic rocks of the Qamdo Block associated with strike-slip faulting, respectively.

In the Lower Pleistocene Wuduizhen Formation, common Cretaceous zircon ages and increasing proportion of metamorphic zircons in the 200–350 Ma population (Fig. 7) suggest provenance from (ultra)high-pressure metamorphic rocks of the Dabie orogenic belt. Specifically, the Early Mesozoic metamorphic zircons (e.g., 219 Ma) yield ages consistent with the exhumation-related (U)HP metamorphism of the Dabie orogen (ca. 223–226 Ma; Zhao and Zheng, 2009; Zhao et al., 2017). The 131 Ma magmatic zircon age peak coincides with the Late-stage magmatic activity of the Dabie orogen, rather than the main anatectic episode of the Sulu orogen (ca. 160–145 Ma; Zhao et al., 2024). This interpretation is further supported by provenance mixing calculations by Tao (2022), which are consistent with a rapid increase in sediment contribution from the Qinling-Dabie orogen.

Three distinct evolutionary phases are indicated by integrated lithofacies analysis and detrital-zircon U-Pb geochronology of the Sure-1 and Sure-2 wells (Fig. 8): 1) *Late Cretaceous to Eocene*: sediment was mainly supplied by proximal intermediate to felsic igneous sources from the Zhangbaling and Sunan uplifts to the south, and next from the Binhai Uplift to the north, with minor contribution from the Qinling–Dabie orogen; 2) *Neogene Yancheng Formation*: the Subei Basin began to receive detritus from the upper Yangtze River catchment, indicating integration into the Paleo-Yangtze system; 3) *Lower Pleistocene Wuduizhen Formation*: substantial input from the Qinling–Dabie orogen is documented, indicating the establishment of the modern Huai River draining both Qinling–Dabie orogen and Yangtze Block.

5.2. Birth and evolution of the Huai River

5.2.1. Phase 1: Late Cretaceous–Paleogene closed basin with proximal sources

Upper Cretaceous to Eocene feldspatho-litho-quartzose sandstones with felsic volcanic lithics and abundant Jurassic–Cretaceous and Neoproterozoic detrital zircons with few 200–350 Ma metamorphic zircons point to proximal sources. Contributions from Neoproterozoic metamorphic and Mesozoic igneous rocks of the Zhangbaling Uplift and from Sinian–Paleozoic carbonates, clastic rocks, and Yanshanian intermediate to felsic igneous rocks of the Sunan Uplift are indicated. Bed-thickness and grain-size trends in sandstones of the Gaoyou Sag independently confirm northward sediment dispersal (Wang and Jiang, 2021a, 2021b). In the Eocene Sanduo Formation, dominance of Permian and Paleoproterozoic zircon ages coupled with an increase in sedimentary lithics at the expense of volcanic lithics testify to a provenance shift toward the Binhai Uplift in the north. Throughout Phase 1, dominance of detritus derived from the surrounding footwall uplifts indicates that the Subei Basin was a hydrologically closed depocenter fed by short local rivers. Such a closed-basin configuration was induced by extensional

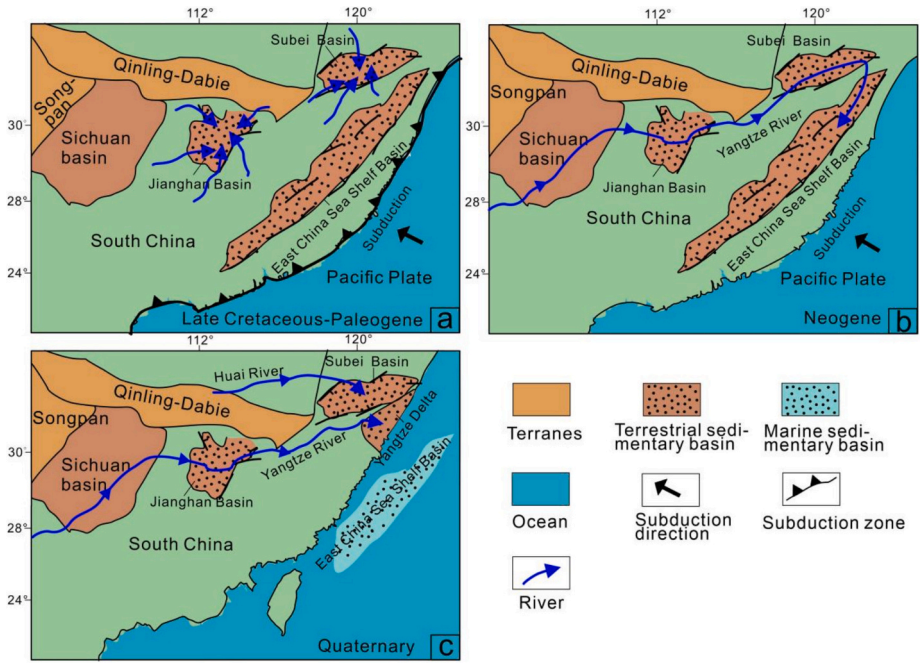

Fig. 8. Cenozoic drainage evolution in southeastern China (mod. after Wang and Jiang, 2021a, 2021b): a) in the Late Cretaceous-Paleogene, back-arc extension led to the development of pull-apart basins where locally fed deltaic to lacustrine sediments were deposited; b) in the Neogene, further subsidence during ongoing subduction of the Pacific Plate opened up a path for the through-going Paleo-lower Yangtze fluvial system; c) in the Quaternary, renewed uplift of the Qinling-Dabie orogen influenced by the ongoing Indo-Asia convergence led to the birth of the modern Huai River.

tectonics leading to the separate development of the Subei, Jianghan, and East China Sea Shelf fault-bound basins in southeast China (Wu et al., 2018; Xu et al., 2021; Fig. 8a). Basin isolation was reinforced by regional uplift in the early Oligocene, which generated a widespread unconformity and removed Oligocene strata across the entire Lower Yangtze basin (Ren et al., 2002; Lee et al., 2006; Zheng et al., 2013).

5.2.2. *Phase 2: Neogene appearance of upper Yangtze-derived detritus*

The Yancheng Formation records a fundamental provenance shift. In addition to the local sources identified above, sample 21SR144 from the Sure-1 Well contains two diagnostic components not observed in underlying strata and absent from all potential proximal sources surrounding the Subei Basin: 1) basaltic lithic fragments comparable to Permian Emeishan basalts exposed along the western margin of the Sichuan Basin; 2) detrital zircons yielding Cenozoic ages and characterized by Th/U > 0.4 and REE patterns indicating magmatic origin, plausibly from felsic igneous products emplaced in the Qamdo Block of the upper Yangtze region during strike-slip faulting (Shang et al., 2024; Yang et al., 2006). The co-occurrence of these two distinct upper Yangtze fingerprints indicates transport from the Jinsha River catchment and therefore initial integration of a Paleo-Yangtze River connecting the upper Yangtze Block to the East Asian continental margin. Such timing is supported by independent constraints: i) paleogeomorphic modeling indicates that the Three Gorges were breached at ~26 Ma (Tian et al., 2024); ii) apatite fission-track and (U-Th)/He thermochronology records initial Three Gorges incision in the late Oligocene to early Miocene (Yang et al., 2023); iii) Nd isotopic evidence from the Red River Delta supports Yangtze River establishment in the late Oligocene (~24 Ma; Clift et al., 2006). The geodynamic trigger for drainage integration was the broad-scale post-rift subsidence of the Subei Basin (Huang and Zhao, 2006; Ma et al., 2019; Fig. 8b). Thermal relaxation and reduced fault activity allowed the basin to evolve from an isolated graben system into a regionally connected depocenter, a topographic configuration essential for capturing a large through-going river (Yao et al., 2017; Zhu et al., 2020).

5.2.3. *Phase 3: Early Pleistocene provenance shift to the Qinling-Dabie orogen*

The most apparent provenance shift is testified by sandstones of the Wuduizhen Formation, where high- to ultrahigh-pressure metamorphic rock fragments appear, and zircons with ages of 200–350 Ma become twice to three-times more abundant (from ~7–12% in older strata to 24%). These zircons are characterized by low Th content (0.4–53.7 ppm) and low Th/U ratios (mostly <0.1), indicative of amphibolite- to granulite-facies metamorphic conditions (Rubatto, 2017). They also show moderate HREE enrichment (Yb_N/Gd_N = 2.0–10.9 vs. typically >20 in magmatic zircon) and no significant Eu anomaly (Eu/Eu* = 0.8–1.2), further supporting a metamorphic origin. Such an increase in Indosinian metamorphic zircons coupled with the first appearance of HP–UHP metamorphic lithics uniquely points to the Dabie orogenic belt (Zheng et al., 2014) and specifically indicates long-distance transport from the Dabie hinterland. Prominent sediment supply from the Qinling-Dabie orogenic belt is consistent with the result of sediment-mixing calculations (Tao, 2022).

The marked provenance shift that took place at ~2.6 Ma testifies to the initial establishment of the modern Huai River. The timing of such a drainage reorganization is consistent with facies transition from Paleogene–Neogene fluvial-lacustrine to Quaternary fluvial-dominated deposition in the intermontane basins of the northern Dabie piedmont (Li et al., 2020) and with initiation of the Qingzang Movement, which triggered renewed uplift and erosion of the Qinling-Dabie orogen (Wang et al., 2022a, 2022b; Fig. 8c).

6. Summary

Provenance analysis of the Upper Cretaceous to Pleistocene sedimentary succession cored by the Sure wells reveals that the Subei Basin experienced two major provenance shifts. The first one, documented at the Paleogene–Neogene transition, is marked by the appearance of detritus sourced from the Jinsha River catchment in the upper Yangtze region, indicating the initial integration of the Paleo-Yangtze River. The second shift took place at the base of the Pleistocene (~2.6 Ma), when

the dominant provenance reverted to a more proximal source, the Qinling-Dabie orogen, signaling the birth of the modern Huai River. These findings provide new constraints on the Cenozoic drainage evolution of eastern China.

Supplementary data to this article can be found online at https://doi.org/10.1016/j.palaeo.2026.113983.

CRediT authorship contribution statement

Yingdi Pan: Writing – original draft, Investigation, Formal analysis. **Tao Deng:** Writing – review & editing, Writing – original draft, Visualization, Validation, Resources, Project administration, Methodology, Investigation, Funding acquisition, Formal analysis, Data curation, Conceptualization. **Junpeng Guan:** Funding acquisition, Data curation. **Lijuan Wang:** Writing – review & editing, Funding acquisition, Formal analysis, Data curation. **Eduardo Garzanti:** Writing – review & editing, Validation, Supervision, Resources, Project administration, Methodology, Investigation, Funding acquisition, Formal analysis, Data curation, Conceptualization. **Xiumian Hu:** Writing – review & editing, Validation, Supervision, Resources, Project administration, Methodology, Investigation, Funding acquisition, Formal analysis, Data curation, Conceptualization.

Declaration of competing interest

The authors declare that they have no known competing financial interests or personal relationships that could have appeared to influence the work reported in this paper.

Acknowledgements

We are grateful for the insightful comments and constructive suggestions by the Editor and two anonymous reviewers. This study was supported by the Carbon Peak and Carbon Neutralization Science and Technology Innovation Special Fund of Jiangsu Province, China (Grants No. BE2022034-1 and BE2022859) and the National Natural Science Foundation of China (Grant No. 42502096).

Data availability

The authors confirm that all data necessary for supporting the scientific findings of this paper have been provided.

References

Cai, L.X., Xiao, G.L., Guo, X.W., Wang, J., Wu, Z.Q., Li, B.G., 2019. Characteristics and main controlling factors of Lower Silurian source rocks in the South Yellow Sea Basin: Insights from marine-continental correlation in the Lower Yangtze region. J. Jilin Univ. (Earth Sci. Ed.) 49, 39–52.

Carroll, A.R., Bohacs, K.M., 1999. Stratigraphic classification of ancient lakes: balancing tectonic and climatic controls. Geology 27, 99–102. https://doi.org/10.1130/0091-7613(1999)027<0099:SCOALB>2.3.CO;2.

Chen, D.L., 2014. Garnet Provenance Tracing of Fluvial Sediments in the Subei Basin since the Late Miocene (Ph.D. Thesis). Nanjing Normal Univ, Nanjing.

Cheng, Y., Li, X.Q., Shu, J.W., Bai, S.B., Zhao, Z.Y., Zhang, X.Y., Guo, G., Zhang, P., Lin, J. X., 2019. Sedimentary evolution and transgressions of the western Subei Basin in Eastern China since the Late Pliocene. Acta Geol. Sin. (Engl. Ed.) 93, 155–166. https://doi.org/10.1111/1755-6724.13777.

Chew, D.M., Petrus, J.A., Kamber, B.S., 2014. U-Pb LA-ICPMS dating using accessory mineral standards with variable common Pb. Chem. Geol. 363, 185–199. https://doi.org/10.1016/j.chemgeo.2013.11.006.

Clift, P.D., Blusztajn, J., Nguyen, A.D., 2006. Large-scale drainage capture and surface uplift in eastern Tibet-SW China before 24 Ma inferred from sediments of the Hanoi Basin, Vietnam. Geophys. Res. Lett. 33, L19403. https://doi.org/10.1029/2006GL027772.

Deng, T., Hu, X., Chew, D., Schönig, J., Ma, A., Liang, W., Drakou, F., 2024. Early Jurassic initiation of the modern drainage pattern of the Dabie orogen (East China) revealed by a multi-proxy provenance approach. Basin Res. 36 (1), e12834.

Gao, W.H., Gao, S., Wang, D.D., Zhao, Y.Y., Zhu, D., Xu, Z., 2015. Information of materials from different rivers recorded in the abandoned Huanghe River sediments: based on analyses of heavy minerals and geochemical elements. Sci. Geogr. Sin. 35, 1631–1639.

Garzanti, E., 2019. Petrographic classification of sand and sandstone. Earth Sci. Rev. 192, 545–563.

He, M.Y., 2014. Provenance Tracing of the Yangtze River Sediments Based on Mineralogy, Geochemistry and Detrital Zircon Geochronology. Nanjing Univ. Press, Nanjing.

Hu, Z.B., Pan, B.T., Bridgland, D., et al., 2017. The linking of the upper-middle and lower reaches of the Yellow River as a result of fluvial entrenchment. Quat. Sci. Rev. 166, 324–338. https://doi.org/10.1016/j.quascirev.2017.02.026.

Huang, J., Zhao, D., 2006. High-resolution mantle tomography of China and surrounding regions. J. Geophys. Res. Solid Earth 111, B09305. https://doi.org/10.1029/2005JB004066.

Ingersoll, R.V., Bullard, T.F., Ford, R.L., Grimm, J.P., Pickle, J.D., Sares, S.W., 1984. The effect of grain size on detrital modes: a test of the Gazzi-Dickinson point-counting method. J. Sediment. Res. 54, 103–116. https://doi.org/10.1306/212F83B9-2B24-11D7-8648000102C1865D.

Jackson, S.E., Pearson, N.J., Griffin, W.L., Belousova, E.A., 2004. The application of laser ablation-inductively coupled plasma-mass spectrometry to in situ U-Pb zircon geochronology. Chem. Geol. 211, 47–69. https://doi.org/10.1016/j.chemgeo.2004.06.017.

Lee, G.H., Kim, B., Shin, K.S., Sunwoo, D., 2006. Geologic evolution and aspects of the petroleum geology of the northern East China Sea shelf basin. AAPG Bull. 90, 237–260. https://doi.org/10.1306/08010505063.

Li, Z.M., Gao, H.S., Liu, F.L., Wang, S., Wu, R.L., Zhang, C.G., 2020. Analysis on the formation age of the Huai River. Prog. Geogr. 39, 1708–1716.

Liang, L.L., 2018. Shallow Geological Structure Characteristics and Three-dimensional Modeling in the Northern Yangzhou Area, Jiangsu Province. M.S. Thesis. China Univ. Pet., Beijing https://doi.org/10.27643/d.cnki.gsybu.2018.001619.

Lin, C.S., Zhang, H.Y., Li, S.T., Ren, J.Y., Zhang, Y.Z., 2004. Episodic rifting dynamic process and quantitative model of Mesozoic-Cenozoic faulted basins in Eastern China. Earth Sci. J. China Univ. Geosci. 29, 583–588.

Liu, F.L., Liou, J.G., 2011. Zircon as the best mineral for P-T-time history of UHP metamorphism: a review on mineral inclusions and U-Pb SHRIMP ages of zircons from the Dabie-Sulu UHP rocks. J. Asian Earth Sci. 40 (1), 1–39. https://doi.org/10.1016/j.jseaes.2010.08.001.

Liu, X.C., Jahn, B.M., Dong, S.W., Lou, Y.X., Cui, J.J., 2008. High-pressure metamorphic rocks from Tongbaishan, central China: U-Pb and $^{40}Ar/^{39}Ar$ age constraints on the provenance of protoliths and timing of metamorphism. Lithos 105 (3–4), 301–318. https://doi.org/10.1016/j.lithos.2008.04.003.

Liu, J.H., Wu, L.F., Qiao, L., Sun, S.Q., Ge, Z.Y., 2014. Soft sediment deformation structures and sedimentary model of the Paleogene Dainan Formation in deep sag of Gaoyou Depression, Subei Basin. Geol. Rev. 60, 1019–1025. https://doi.org/10.16509/j.georeview.2014.05.007.

Ma, P., Liu, S., Gurnis, M., Zhang, B., 2019. Slab horizontal subduction and slab tearing beneath East Asia. Geophys. Res. Lett. 46, 5161–5169. https://doi.org/10.1029/2018GL081703.

Paton, C., Woodhead, J.D., Hellstrom, J.C., Hergt, J.M., Greig, A., Maas, R., 2010. Improved laser ablation U-Pb zircon geochronology through robust downhole fractionation correction. Geochem. Geophys. Geosyst. 11, Q0AA06. https://doi.org/10.1029/2009GC002618.

Peng, J.N., Qiu, Q., Wang, D.Y., Li, Z.M., Zhu, J.H., Liang, S.Y., Wu, Y.L., 2020. Occurrence state and recoverability of tight oil in the Paleogene Funing Formation, Subei Basin. Pet. Geol. Exp. 42, 53–59.

Qiu, X.M., Liu, Y.R., Fu, Q., 2006a. Sequence Stratigraphy and Sedimentary Evolution of Cretaceous to Tertiary in Subei Basin. Geological Publishing House, Beijing, pp. 17–21 (in Chinese).

Qiu, H.J., Xu, Z.Q., Qiao, D.W., 2006b. Research progress on tectonic evolution of the Subei Basin. Geol. Bull. China 25, 1117–1122.

Ren, J., Tamaki, K., Li, S., Zhang, J.X., 2002. Late Mesozoic and Cenozoic rifting and its dynamic setting in Eastern China and adjacent areas. Tectonophysics 344, 175–205. https://doi.org/10.1016/S0040-1951(01)00271-2.

Rubatto, D., 2017. Zircon: the metamorphic mineral. Rev. Mineral. Geochem. 83, 261–295. https://doi.org/10.2138/rmg.2017.83.9.

Shang, F., Weislogel, A., Robinson, D., Zhou, J., Li, R., Liu, S., 2024. Mesozoic evolution of the southeastern Tibetan Plateau from sediment provenance of the Qamdo Basin: implications for proto-plateau development. Tectonics 43, e2023TC008242.

Sharman, G.R., Sharman, J.P., Sylvester, Z., 2018. DetritalPy: a Python-based toolset for visualizing and analysing detrital geo-thermochronologic data. Depos. Rec. 4, 202–215. https://doi.org/10.1002/dep2.45.

Shi, X., Yang, Z., Dong, Y., Zhou, B., 2019. Tectonic uplift of the northern Qinling Mountains (Central China) during the late Cenozoic: evidence from DEM-based geomorphological analysis. J. Asian Earth Sci. 184, 104005. https://doi.org/10.1016/j.jseaes.2019.104005.

Shu, L.S., Wang, B., Wang, L.S., Lu, H.F., Guo, L.Z., 2005. Analysis of Late Cretaceous-Neogene prototype basin in the Subei Basin. Geol. J. China Univ. 11, 534–543. https://doi.org/10.16108/j.issn1006-7493.2005.04.009.

Shu, Q., Zhao, Z., Zhao, Y., Chen, Y., Zhang, M., 2021. Magnetic properties of late Cenozoic sediments in the Subei Basin: implications for the Yangtze River run-through time. J. Coast. Res. 37, 122–131. https://doi.org/10.2112/JCOASTRES-D-20-00003.1.

Sun, S.S., McDonough, W.F., 1989. Chemical and isotopic systematics of oceanic basalts: implications for mantle composition and processes. In: Saunders, A.D., Norry, M.J. (Eds.), Magmatism in the Ocean Basins, 42. Geol. Soc. London Spec. Publ, pp. 313–345. https://doi.org/10.1144/GSL.SP.1989.042.01.19.

Tao, K.J., 2022. Provenance Analysis of Cenozoic Sediments from Borehole GYN1 in the Subei Basin and its Implications for the Yangtze River Connection (Ph.D. Dissertation). China Univ. Geosci., Wuhan.

Tian, Z., Suo, Y., Ding, X., et al., 2024. Cenozoic surface Earth system evolution and dynamic paleogeomorphic reconstruction from the Tibet Plateau to the Western Pacific linked by the Yangtze River. J. Geol. Soc. London 181. https://doi.org/10.1144/jgs2023-183 jgs2023-183.

Tregear, T., 1965. A Geography of China. Univ. London Press, London.

Van Maren, D.S., Winterwerp, J.C., Wang, Z.Y., Pu, Q., 2009. Suspended sediment dynamics and morphodynamics in the Yellow River, China. Sedimentology 56, 785–806. https://doi.org/10.1111/j.1365-3091.2008.00997.x.

Wang, X.Y., Jiang, Z.X., 2021a. Provenance characteristics and tectonic setting analysis of the 3rd Member of the Paleogene Funing Formation, Subei Basin. Earth Sci. Front. 28 (2), 376–390. https://doi.org/10.13745/j.esf.sf.2020.6.31.

Wang, X.Y., Jiang, Z.X., 2021b. Geochemical characteristics of trace elements and rare earth elements of the third member of Paleogene Funing Formation in Dongtai Depression, Subei Basin and their geological significance. Geol. Rev. 67, 355–366. https://doi.org/10.16509/j.georeview.2021.02.006.

Wang, Y., Zhang, Z., Zhu, D., Yang, J., Mao, L., Li, S., 2006. River-sea interaction and the north Jiangsu plain formation. Quat. Sci. 26, 301–320.

Wang, B., Liang, X.P., Zhou, J., 2008. Analysis on relationship between fault activity and earthquakes in Jiangsu Province and its adjacent areas. Plateau Earthquake Res. 20, 38–43.

Wang, Y., Li, C., Hao, Y., Zheng, D., Zhang, H., Yu, J., Pang, J., 2022a. Multi-stage growth in the north margin of the Qinling Orogen, Central China, revealed by both low-temperature thermochronology and river profile inversion. Tectonics 41 (4), e2021TC007029. https://doi.org/10.1029/2021TC007029.

Wang, P., Zheng, H., Wang, Y., Wei, X., Tang, L., Jourdan, F., Chen, J., Huang, X., 2022b. Sedimentology, geochronology, and provenance of the late Cenozoic "Yangtze Gravel": implications for Lower Yangtze River reorganization and tectonic evolution in southeast China. GSA Bull. 134, 463–486. https://doi.org/10.1130/B35862.1.

Wang, J., He, J., Zhao, J., Liu, C., Huang, S., 2023a. Multiple-stage Neoproterozoic magmatism recorded in the Zhangbaling uplift of the Northeastern Yangtze Block: evidence from zircon ages and geochemistry. Minerals 13, 562. https://doi.org/10.3390/min13040562.

Wang, G., Li, S., Suo, Y., Peng, G., Wang, P., Cheng, H., Zhu, M., 2023b. Cenozoic source-to-sink driven by tectono-geomorphic evolution: a systematic detrital zircon U-Pb analysis in the central northern South China Sea. Earth Sci. Rev. 239, 104365. https://doi.org/10.1016/j.earscirev.2023.104365.

Wu, L., Mei, L., Paton, D.A., Guo, P., Liu, Y., Luo, J., Wen, H., 2018. Deciphering the origin of the Cenozoic intracontinental rifting and volcanism in eastern China using integrated evidence from the Jianghan Basin. Gondw. Res. 64, 67–83. https://doi.org/10.1016/j.gr.2018.06.009.

Xiang, W., Griffin, W.L., Jie, C., Pinyun, H., Xiang, L., 2011. U and Th contents and Th/U ratios of zircon in felsic and mafic magmatic rocks: improved zircon-melt distribution coefficients. Acta Geol. Sin. (Engl. Ed.) 85, 164–174. https://doi.org/10.1111/j.1755-6724.2011.00387.x.

Xiong, J., Zhang, P., Deng, C., Picotti, V., Liang, H., Ren, Z.K., Wang, W.T., et al., 2024. Neogene–Quaternary channel evolution and provenance shift of the middle Yellow River. J. Geophys. Res. Earth Surf. 129, e2023JF007532. https://doi.org/10.1029/2023JF007532.

Xu, X., Zuza, A.V., Chen, L., Zhu, W., Yin, A., Fu, X., Yang, S., 2021. Late Cretaceous to early Cenozoic extension in the Lower Yangtze region (East China) driven by Izanagi-Pacific plate subduction. Earth Sci. Rev. 221, 103790. https://doi.org/10.1016/j.earscirev.2021.103790.

Xu, L., Lin, W., Jolivet, M., Chen, Y., Wang, F., Li, Q., 2022. Apatite (U-Th)/He thermochronology evidence for two Cenozoic denudation events in the eastern part of the Sulu orogenic belt. Earth Sci. 47, 1–16.

Yakymchuk, C., Kirkland, C.L., Clark, C., 2018. Th/U ratios in metamorphic zircon. J. Metam. Geol. 36, 715–737. https://doi.org/10.1111/jmg.12307.

Yang, Q., Chen, H.Y., 2003. Tectonic evolution of the North Jiangsu-South Yellow Sea Basin. Pet. Geol. Exp. 25, 562–565.

Yang, S., Li, C., Cai, J., 2006. Geochemical compositions of core sediments in eastern China: implication for Late Cenozoic palaeoenvironmental changes. Palaeogeogr. Palaeoclimatol. Palaeoecol. 229 (4), 287–302. https://doi.org/10.1016/j.palaeo.2005.06.026.

Yang, C., Jiao, R., Zattin, M., et al., 2023. Late Oligocene–early Miocene incision of the Three Gorges and the initial establishment of an east-flowing Yangtze River. Geomorphology 441, 108897. https://doi.org/10.1016/j.geomorph.2023.108897.

Yao, X., Liu, S., Bai, Y., Ji, H., 2017. Neogene residual subsidence and its response to a sinking slab in the deep mantle of eastern China. J. Asian Earth Sci. 143, 269–282. https://doi.org/10.1016/j.jseaes.2017.03.032.

Yu, F., Chen, Z., Ren, X., Yang, G., 2009. Analysis of historical floods on the Yangtze River, China: Characteristics and explanations. Geomorphology 113, 210–216. https://doi.org/10.1016/j.geomorph.2009.03.008.

Zhang, Z.J., 2016. Late Cenozoic Detrital K-Feldspar Pb Isotopic Composition in the Yangtze River Drainage. Ph.D. thesis. China University of Geosciences.

Zhang, L., Liu, J.Q., Qin, X.G., et al., 2018. Magnetostratigraphy and paleoenvironmental events recorded in a late Cenozoic sedimentary succession in Huaibei Plain, East China. Quat. Sci. Rev. 200, 52–64. https://doi.org/10.1016/j.quascirev.2018.09.041.

Zhao, Z.F., Zheng, Y.F., 2009. Remelting of subducted continental lithosphere: Petrogenesis of Mesozoic magmatic rocks in the Dabie-Sulu orogenic belt. Sci. China Ser. D Earth Sci. 52 (9), 1295–1318. https://doi.org/10.1007/s11430-009-0135-9.

Zhao, Z.F., Liu, Z.B., Chen, Q., 2017. Melting of subducted continental crust: Geochemical evidence from Mesozoic granitoids in the Dabie-Sulu orogenic belt, east-central China. J. Asian Earth Sci. 145, 260–277. https://doi.org/10.1016/j.jseaes.2017.03.038.

Zhao, Y., Zhou, G., Chang, H., Zhuang, Y., Hu, P., Wu, Y., 2024. Zircon petrochronological evidences for diachronous tectonic switch and orogenic keel collapse of the Tongbai-Dabie-Sulu orogens. Lithos 480-481, 107639.

Zheng, H., Clift, P.D., Wang, P., Tada, R., Jia, L., He, M., Jourdan, F., 2013. Pre-Miocene birth of the Yangtze River. Proc. Natl. Acad. Sci. U. S. A. 110, 7556–7561. https://doi.org/10.1073/pnas.1216241110.

Zheng, J.P., Tang, H.Y., Xiong, Q., Griffin, W.L., O'Reilly, S.Y., Pearson, N.J., 2014. Linking continental deep subduction with destruction of a cratonic margin: strongly reworked North China SCLM intruded in the Triassic Sulu UHP belt. Contrib. Mineral. Petrol. 168, 1028. https://doi.org/10.1007/s00410-014-1028-0.

Zheng, Y.F., Zhao, Z.F., Chen, R.X., 2019. Ultrahigh-pressure metamorphic rocks in the Dabie–Sulu orogenic belt: compositional inheritance and metamorphic modification. Geol. Soc. Lond. Spec. Publ. 474 (1), 89–132. https://doi.org/10.1144/SP474-2017-240.

Zhou, L.Y., Liu, J., Saito, Y., Zhang, Z.X., Chun, H.X., Hu, G., 2014. Coastal erosion as a major sediment supplier to continental shelves: example from the abandoned Old Huanghe (Yellow River) delta. Cont. Shelf Res. 82, 43–59. https://doi.org/10.1016/j.csr.2014.04.004.

Zhu, X.F., Shen, C.B., Zhou, R.J., Xu, J.Y., Zhao, J.X., Wang, L., Ge, X., 2020. Paleogene sediment provenance and paleogeographic reconstruction of the South Yellow Sea Basin, East China: constraints from detrital zircon U-Pb geochronology and heavy mineral assemblages. Palaeogeogr. Palaeoclimatol. Palaeoecol. 553, 109776. https://doi.org/10.1016/j.palaeo.2020.109776.

Zuo, Z.J., Wang, X.K., Cheng, S.P., Luo, W.J., Wang, W.F., 2006. Sediment regulation of the quaternary stratum in the Drainage Basin of Huai River (Henan Section). Ground Water 28, 34–36.